Moderate excess of pyruvate augments osteoclastogenesis

Jenna E. Fong[1,*], Damien Le Nihouannen[1,*,‡], Kerstin Tiedemann[1,2], Gulzhakhan Sadvakassova[1,2], Jake E. Barralet[1] and Svetlana V. Komarova[2,1,§]

[1]Faculty of Dentistry, McGill University, Montreal, QC H3A 1A4, Canada
[2]Shriners Hospital for Children – Canada, Montreal, QC H3G IA6, Canada

*These authors contributed equally to this work
‡Present address: INSERM U1026, BioTiS – Tissue Engineering, Université Victor Segalen Bordeaux 2, Zone Nord, Bâtiment 4A – case postale 45, 146 rue Léo Saignat, 33076 Bordeaux Cedex, France
§Author for correspondence (svetlana.komarova@mcgill.ca)

Biology Open 2, 387–395
doi: 10.1242/bio.20133269
Received 2nd October 2012
Accepted 18th January 2013

Summary

Cell differentiation leads to adaptive changes in energy metabolism. Conversely, hyperglycemia induces malfunction of many body systems, including bone, suggesting that energy metabolism reciprocally affects cell differentiation. We investigated how the differentiation of bone-resorbing osteoclasts, large polykaryons formed through fusion and growth of cells of monocytic origin, is affected by excess of energy substrate pyruvate and how energy metabolism changes during osteoclast differentiation. Surprisingly, small increases in pyruvate (1–2 mM above basal levels) augmented osteoclastogenesis *in vitro* and *in vivo*, while larger increases were not effective *in vitro*. Osteoclast differentiation increased cell mitochondrial activity and ATP levels, which were further augmented in energy-rich conditions. Conversely, the inhibition of respiration significantly reduced osteoclast number and size. AMP-activated protein kinase (AMPK) acts as a metabolic sensor, which is inhibited in energy-rich conditions. We found that osteoclast differentiation was associated with an increase in AMPK levels and a change in AMPK isoform composition. Increased osteoclast size induced by pyruvate (1 mM above basal levels) was prevented in the presence of AMPK activator 5-amino-4-imidazole carboxamide ribonucleotide (AICAR). In keeping, inhibition of AMPK using dorsomorphin or siRNA to AMPKγ increased osteoclast size in control cultures to the level observed in the presence of pyruvate. Thus, we have found that a moderate excess of pyruvate enhances osteoclastogenesis, and that AMPK acts to tailor osteoclastogenesis to a cell's bioenergetics capacity.

Key words: Hyperglycemia, Pyruvate, Osteoclastogenesis, ATP, AMPK

Introduction

Diabetes mellitus is a widespread group of metabolic diseases characterized by high blood glucose levels (Wild et al., 2004). Complications of diabetes affect many organs including bone, where diabetes is associated with changes in bone mineral density (Nicodemus and Folsom, 2001), an increased fracture risk (Khazai et al., 2009), and a delayed fracture repair (Kayal et al., 2007). These problems are most pronounced in hyperglycemic patients, but are mostly relieved if glucose is well controlled. Thus, elevated glucose levels impact the quality of bone tissue. In addition to glucose, other bioenergetics substrates, such as pyruvate, can be utilized by osteoclasts; however, their effect on osteoclastogenesis is not known.

Bone homeostasis is maintained by a balance between bone resorption by osteoclasts and bone formation by osteoblasts. Osteoclasts are terminally differentiated multinucleated cells formed by the fusion of hematopoietic precursors. Osteoclast differentiation and function demands significant increase in energy consumption, which is required for monocyte proliferation and fusion, protein synthesis to gain resorptive machinery, and activity of homeostatic and resorptive ion pumps. In keeping, exposure of monocytes to pro-resorptive cytokine receptor activator of NF-κB ligand (RANKL) results in increased glucose and oxygen consumption (Kim et al., 2007), upregulation of Krebs cycle and oxidative phosphorylation enzymes (Czupalla et al., 2005), and the production of abundant mitochondria (Dudley and Spiro, 1961). Moreover, mitochondrial biogenesis has been shown to be critical for osteoclast formation (Ishii et al., 2009), resulting in a marked increase in ATP levels during osteoclastogenesis (Le Nihouannen et al., 2010). Thus, addition of substrates utilized for oxidative phosphorylation, such as Krebs cycle intermediates, can potentially affect osteoclastogenesis. However, it remains unclear how energy-expensive osteoclastogenesis adapts to and is regulated by different metabolic substrates.

Metabolic sensors are capable of detecting the cell metabolic status and communicating it to functional signaling pathways. AMP-activated protein kinase (AMPK) is stimulated by an increase in the AMP/ATP ratio, which signifies cell inability to cope with the energy demand (Finley and Haigis, 2009). AMPK acts both to decrease current metabolic expenditure and to improve energy production. Recently, RANKL-induced AMPK activation has been shown to negatively regulate osteoclast

differentiation (Lee et al., 2010), but relationship between osteoclast bioenergetics and metabolic sensors has not been addressed.

The aim of this study was to explore the interaction between homeostatic and functional signaling in osteoclasts in the presence of excessive amounts of pyruvate. To assess osteoclastogenesis *in vitro*, we differentiated osteoclasts from mouse bone marrow cells and from mouse monocytic RAW 264.7 cell line. To confirm our findings *in vivo*, we used healthy mice injected with pyruvate. Surprisingly, we have found that independently of the model used and basal levels of energy substrates, moderate excess of pyruvate significantly augmented osteoclastogenesis.

Results

Excess of pyruvate augments osteoclastogenesis *in vitro* and *in vivo*

We first supplemented RAW 264.7 culture media with pyruvate (1 mM) and assessed osteoclastogenesis. We have found that addition of pyruvate significantly augmented the formation of giant osteoclast-like cells induced by RANKL (Fig. 1A). Appearance of osteoclastic cells in pyruvate-treated cultures suggests changes in cell size as well as number. Using confocal microscopy (Fig. 1B), we confirmed that osteoclast height was not significantly different, 22.2±1.9 µm in control cultures and 23.7±2.9 µm in pyruvate-treated cultures, indicating that change in osteoclast planar area can be used as a measure of osteoclast size. Extended analysis of osteoclastic cells generated in the presence of pyruvate indicated significant increase in the number of giant cells formed in the presence of RANKL (Fig. 1C), in the osteoclast size as estimated by cell planar surface area, (Fig. 1D), in the number of nuclei per osteoclast-like cell (Fig. 1E) and the cell surface per nucleus (Fig. 1F). Addition of pyruvate significantly increased osteoclast numbers only when added at low concentrations, 1–2 mM, while higher concentrations, 3–4 mM were not effective (Fig. 1G). To assess if osteoclast-stimulatory effect was unique to addition of pyruvate, we used another Krebs cycle intermediate citrate, and demonstrated that it similarly and significantly increases osteoclastogenesis (Fig. 1H).

RAW 264.7 cells were originally established from a tumor induced by Abelson murine leukemia virus, and the standard culture medium for RAW 264.7 cells, DMEM, contains 25 mM glucose,

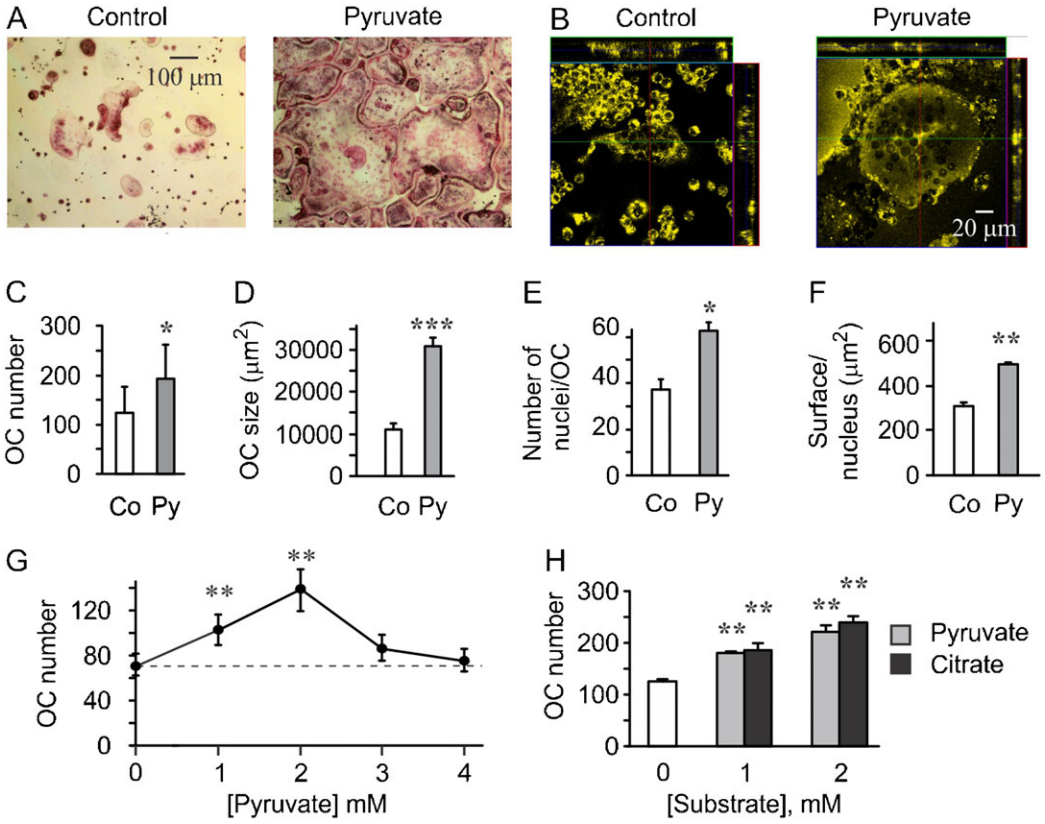

Fig. 1. Osteoclast differentiation from RAW 264.7 cells is augmented by excess in pyruvate. (**A–F**) RAW 264.7 cells were cultured in supplemented DMEM containing 25 mM basal glucose and treated with RANKL (50 ng/ml) for 4 days in the absence or presence of pyruvate (Py, 1 mM). (A) Representative images of osteoclasts generated in control cultures and in pyruvate-treated cultures. Scale bar: 100 µm applies to both images. (B) Confocal images of osteoclasts generated from RAW 264.7 cells in the absence or presence of pyruvate and stained with lipophilic membrane probe DiI. Scale bar: 20 µm applies to both images. (C) Average number of osteoclasts formed in control and pyruvate-treated cultures. (D) Average osteoclast surface area. (E) Average number of nuclei per osteoclast. (F) Average surface area per nucleus. For C–F, data are means ± s.e.m.; $n=6$ independent experiments. Statistical significance compared to control was assessed by paired *t*-test, $*P<0.05$; $**P<0.01$; $***P<0.001$. (**G**) RAW 264.7 cells were cultured with RANKL (50 ng/ml) for 4 days without additions (untreated, dashed line) or in the presence of pyruvate (1–4 mM) and osteoclast numbers were assessed. Data are means ± s.e.m.; $n=8$ independent experiments; $**P<0.01$ was assessed by ANOVA for correlated samples followed by Tukey post-test. (**H**) RAW 264.7 cells were cultured with RANKL (50 ng/ml) for 4 days without additions (open bar) or in the presence of 1–2 mM of pyruvate (gray bars) or citrate (black bars) and osteoclast numbers were assessed. Data are means ± s.e.m.; $n=3$ independent experiments, $**P<0.01$ was assessed by ANOVA for correlated samples followed by Tukey post-test.

therefore we assessed if the observed effect of pyruvate on osteoclastogenesis may be limited to this cell line and culture conditions only. We added pyruvate (1 mM) to two types of primary osteoclastogenesis cultures: i) non-adherent mouse bone marrow cells (NaBMC) treated with RANKL (100 ng/ml) and M-CSF (50 ng/ml) at 5 mM basal glucose and 1 mM basal pyruvate (Fig. 2A), and ii) mouse bone marrow cells treated with ascorbic acid (AA) (50 µg/ml) and RANKL (50 ng/ml) at 5 mM basal glucose (Fig. 2B). Similar to the effect of pyruvate on RAW 246.7 cells, addition of pyruvate to primary osteoclast cultures significantly increased the number of osteoclasts formed in the presence of osteoclastogenic factors (Fig. 2C), the osteoclast size as estimated by cell planar surface area, (Fig. 2D), the number of nuclei per osteoclast (Fig. 2E) and the cell surface per nucleus (Fig. 2F).

To assess if pyruvate affects osteoclast functional activity, we performed an *in vitro* pit formation assay. RAW 264.7 cells were plated on calcium phosphate resorbable substrates and cultured with or without pyruvate for 7 days (Fig. 3A). We have found that the presence of pyruvate resulted in significant increase in area of pits formed by resorption of individual osteoclastic cells (Fig. 3B), and the total area resorbed that reflects both the number and the size of individual pits (Fig. 3C), indicating an increase in resorptive activity of osteoclastic cells formed in energy-rich conditions. Similarly, in primary osteoclast cultures we have found that exposure to pyruvate significantly augmented expression of osteoclastic genes necessary for resorptive activity, proteases cathepsin K and MMP-9, as well as osteoclast marker gene calcitonin receptor (Fig. 3D).

We next examined if small excess of pyruvate can affect osteoclastogenesis *in vivo*. We injected healthy mice with pyruvate (0.75 g/kg/day) for 7 days and examined multinucleated TRAP-positive osteoclasts in long bones (Fig. 4A). In healthy animals, such injections are known to lead to a short-term, 20–40 minutes, increase in blood levels of pyruvate (Fukushima et al., 2009). We analyzed the steady-state levels of pyruvate and glucose in vehicle- or pyruvate-injected mice. While, as expected in well-controlled healthy animals, we did not observe significant change in blood pyruvate levels (Fig. 4B), the levels of glucose were significantly lower in pyruvate-treated mice (Fig. 4C). We have found that mild excess in pyruvate did not affect osteoclast number (Fig. 4D), but significantly increased the osteoclast surface area/bone area (Fig. 4E), indicating the formation of larger osteoclasts.

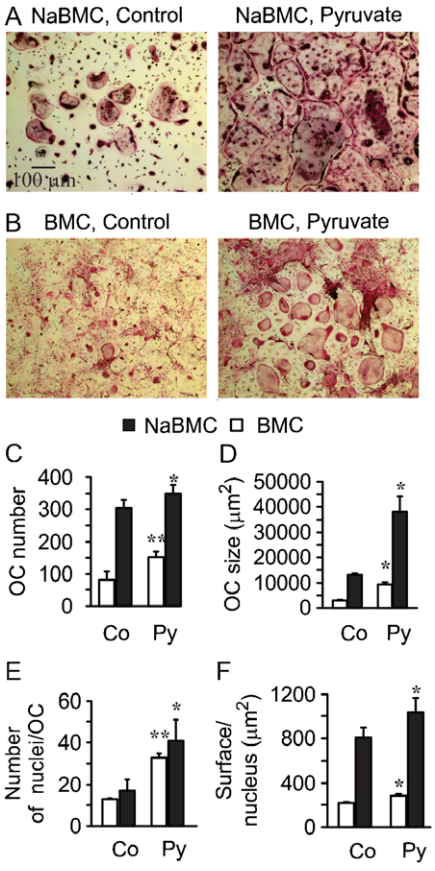

Fig. 2. Osteoclast differentiation from bone marrow cells is augmented by pyruvate. (**A**) Representative images of non-adherent bone marrow cells cultured in supplemented α-MEM containing 5 mM basal glucose and 1 mM basal pyruvate with RANKL (100 ng/ml) and M-CSF (50 ng/ml) for 4 days (NaBMC) without (Control) or with additional pyruvate (1 mM). Scale bar: 100 µm applies to all images. (**B**) Representative images of mouse bone marrow cells cultured in supplemented MEM containing 5 mM basal glucose with AA (50 µg/ml) and RANKL (50 ng/m) for 4 days (BMC) without (Control) or with pyruvate (1 mM). (**C**) Average number of osteoclasts formed in control or pyruvate-treated NaBMC (black bars) and BMC (white bars) cultures. (**D**) Average osteoclast surface area. (**E**) Average number of nuclei per osteoclast. (**F**) Average surface area per nucleus. For C–F, data are means ± s.e.m.; $n=3$ independent experiments for NaBMC, $n=4$ for BMC, $^{*}P<0.05$; $^{**}P<0.01$ compared to samples cultured at standard conditions was assessed by paired *t*-test.

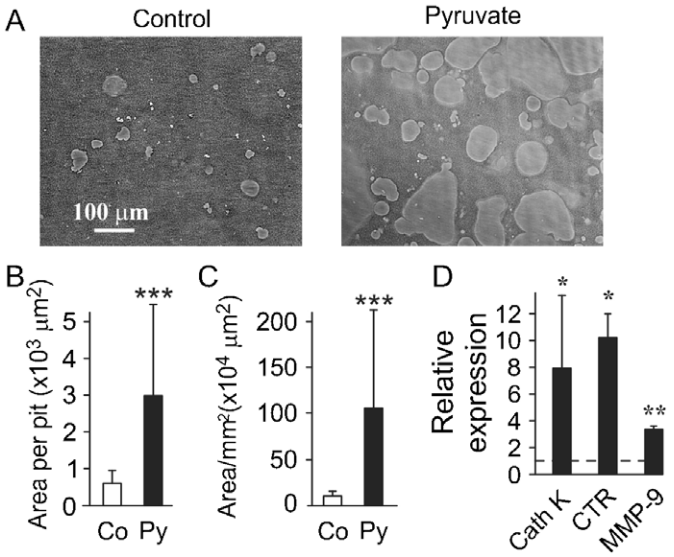

Fig. 3. Osteoclasts formed in the presence of pyruvate exhibit higher resorptive activity. (**A–C**) RAW 264.7 cells were plated on calcium phosphate and cultured for 10 days with RANKL (50 ng/ml) without or with pyruvate (1 mM, Py). (A) Representative images of resorption pits in control cultures (left) and cultures treated with pyruvate (right). Scale bar: 100 µm applies to both images. (B) Average area of a single resorption pit. (C) Average total resorption area per 1 mm^2 of substrate. Data are means ± s.d., $n=20$ fields per condition, $^{***}P<0.001$ indicates significance assessed by *t*-test. (**D**) Non-adherent bone marrow cells were treated with RANKL (100 ng/ml) and M-CSF (50 ng/ml) for 4 days in the presence or absence of pyruvate, and the expression of cathepsin K (CathK), calcitonin receptor (CTR) and MMP-9 was assessed. Data are means ± s.e.m., $n=3$–6 independent experiments, $^{*}P<0.05$; $^{**}P<0.01$; indicate significance assessed by *t*-test.

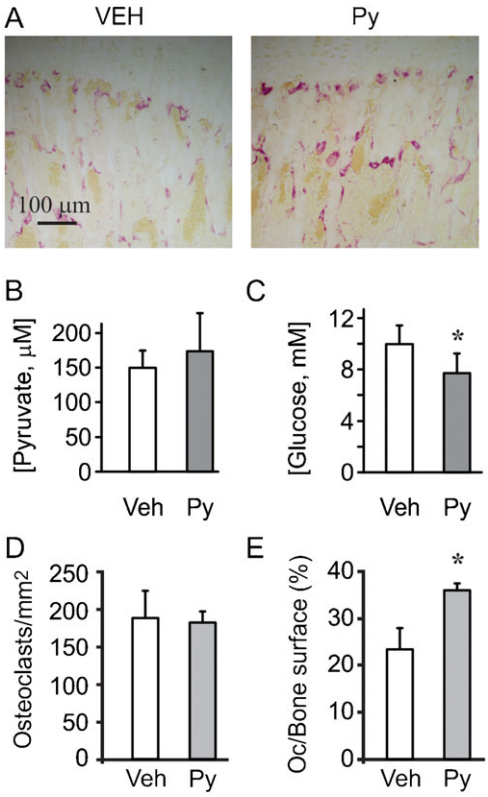

Fig. 4. Pyruvate augments osteoclastogenesis *in vivo*. Mice were injected for 7 days with pyruvate (0.75 g/kg/day). Osteoclast number and surface were assessed on paraffin-embedded sections from proximal tibiae. (**A**) Representative images of osteoclasts in vehicle-treated (left), and pyruvate-treated (right) bones. Scale bar: 100 μm applies to both images. (**B**,**C**) Basal blood levels of pyruvate (B) and glucose (C) in mice injected with vehicle or pyruvate. Data are means ± s.d., $n=6$ animals per condition, statistical significance was assessed by *t*-test, $*P<0.05$. (**D**) Average number of osteoclasts per mm^2. (**E**) Average osteoclast surface per bone surface. Data are means ± s.e.m., $n=3$ animals (3 sections/animal), statistical significance was assessed by *t*-test, $*P<0.05$.

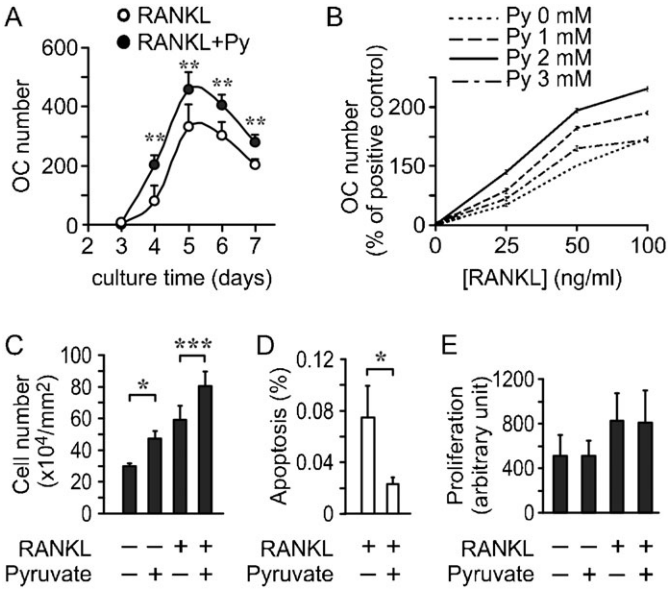

Fig. 5. Effect of pyruvate on osteoclast precursors. (**A**) RAW 264.7 cells were cultured with RANKL, without (white circles) or with pyruvate (1 mM, black circles) and osteoclast numbers formed on days 3–7 were assessed. Data are means ± s.e.m., $n=3$–5 independent experiments, $**P<0.01$ indicates significance for the effect of pyruvate assessed by two-way ANOVA, which indicated significant influence of both time and pyruvate treatment. (**B**) Effect of pyruvate on osteoclast formation was pyruvate concentration- and RANKL concentration-dependent. For each pyruvate concentration (Py, 0, 1, 2 and 3 mM), RAW 264.7 cells were treated with 0, 25, 50 or 100 ng/ml of RANKL for 4 days. Osteoclast number was assessed for each condition and normalized to number of osteoclasts formed with 50 ng/ml of RANKL without pyruvate. (**C**,**D**) RAW 264.7 cells were cultured for 2 days with RANKL, without or with pyruvate, and the samples were fixed and stained with DAPI. The number of pre-osteoclasts (C) and the proportion of cells exhibiting nuclear fragmentation (D) were assessed. Data are means ± s.e.m., $n=3$ independent experiments, $*P<0.05$; $***P<0.001$ indicate significance assessed by *t*-test. (**E**) RAW 264.7 cells were cultured for 4 days with or without RANKL and in the absence or presence of pyruvate (1 mM). BrdU incorporation was assessed in each condition. Data are means ± s.e.m. of $n=6$ independent experiments, no statistically significant difference.

Effects of excess pyruvate on osteoclast precursors

In vitro, pyruvate augmented osteoclast formation at all time points (Fig. 5A), and had qualitatively similar effects at different levels of RANKL (Fig. 5B). We examined if pyruvate affects osteoclast precursors, and found that both in untreated and RANKL-treated cultures, addition of pyruvate significantly increased the precursor cell density (Fig. 5C). This effect was due to decrease in the proportion of apoptotic precursors in the presence of pyruvate (Fig. 5D), while precursor proliferation was unaffected by pyruvate (Fig. 5E).

Pyruvate-induced increase in osteoclast metabolic activity is critical for regulation of cell growth

Since pyruvate was previously suggested to exhibit anti-oxidant properties (Bassenge et al., 2000; Mohanty et al., 2002), we first examined its effect on the osteoclast redox status. In keeping with our previous studies (Le Nihouannen et al., 2010), we have found that osteoclast differentiation resulted in a decrease in total glutathione and the ratio of reduced glutathione (GSH) to oxidized glutathione (GSSG). Addition of pyruvate did not affect the total glutathione content (Fig. 6A), and only slightly increased a GSH/GSSG ratio (Fig. 6B).

We next examined the effect of pyruvate on osteoclast energy metabolism. Treatment of RAW 264.7 with RANKL induced significant media acidification, which was dramatically increased in the presence of pyruvate (Fig. 7A). Lactate exhibited an overall trend to increase in the presence of RANKL and pyruvate,

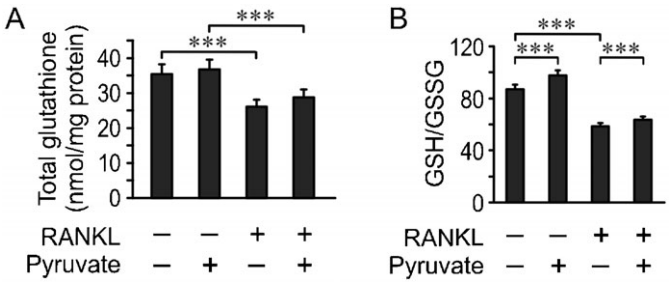

Fig. 6. Effect of pyruvate on osteoclast redox status. RAW 264.7 cells were cultured for 4 days with or without RANKL and in the absence or presence of pyruvate (1 mM). Total glutathione (GSH+GSSG) levels (**A**) and GSH/GSSG ratio (**B**) were assessed. Data are means ± s.e.m., $n=5$ independent experiments, $***P<0.001$ indicates significance assessed by *t*-test.

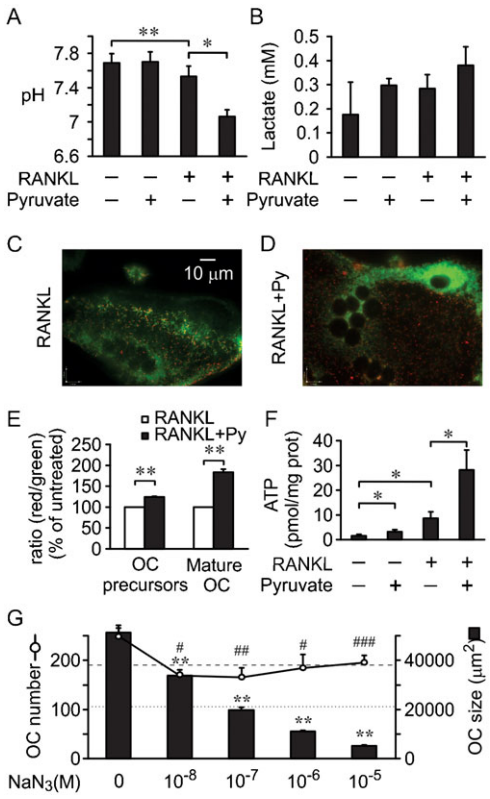

Fig. 7. Effect of pyruvate on osteoclast energy metabolism. RAW 264.7 cells were cultured for 2 days (OC precursors) or 4 days (mature OC) with or without RANKL and with or without pyruvate (1 mM). (**A**,**B**) Media pH (A), and lactate concentration (B) were assessed. Data are means ± s.e.m., $n=3$ independent experiments, $^{*}P<0.05$; $^{**}P<0.01$ indicate significance assessed by paired *t*-test. (**C**,**D**) Representative images of mitochondria stained with the vital mitochondrial dye JC-1 in osteoclasts formed in the presence of RANKL alone (C) or RANKL and pyruvate (D). Scale bar: 10 μm applies to both images. (**E**) Mitochondrial transmembrane potential $\Delta\psi_m$ (indicated by red to green intensity ratios of JC-1) normalized to the ratio obtained in cultures treated with RANKL only. Data are means ± s.e.m., $n=3$ independent experiments, $^{**}P<0.01$ indicates significance assessed by *t*-test. (**F**) Intracellular ATP concentration. Data are means ± s.e.m., $n=4$ independent experiments, $^{*}P<0.05$ indicates significance assessed by paired *t*-test. (**G**) RAW 264.7 cells were cultured with RANKL and pyruvate in the presence of increasing concentration of NaN_3, and osteoclast number and size were assessed. Dashed line indicates osteoclast number and dotted line indicates osteoclast size in cultures treated with RANKL only. Data are means ± s.e.m., $n=3$ independent experiments, *indicates significance for cell size and #for cell numbers, compared to samples cultured without NaN_3, $^{i}P<0.05$; $^{ii}P<0.01$; $^{iii}P<0.001$ indicate significance assessed by ANOVA.

which did not reach statistical significance (Fig. 7B). To assess changes in oxidative phosphorylation we examined mitochondrial activity of osteoclast precursors and mature osteoclast-like cells using live cell mitochondrial transmembrane potential ($\Delta\psi_m$) indicator JC-1. At low $\Delta\psi_m$, JC-1 forms monomers emitting green fluorescence, at high $\Delta\psi_m$ JC-1 aggregates, shifting to red fluorescence (Fig. 7C,D). Treatment with pyruvate increased $\Delta\psi_m$ both in osteoclast precursors and, more dramatically, in mature osteoclastic cells (Fig. 7E). We next evaluated the intracellular ATP concentration ([ATP]). Treatment of RAW 264.7 cells with RANKL induced a significant 5-fold increase in [ATP], and addition of pyruvate during osteoclastogenesis resulted in a further 3-fold increase in [ATP] (Fig. 7F). To assess how impeding energy production affects osteoclast differentiation, we treated the cultures with low concentrations of respiration inhibitor NaN_3. Treatment with NaN_3 significantly and dose-dependently reduced both the number and the size of osteoclastic cells formed in the presence pyruvate (Fig. 7G). Whereas cell numbers were reduced to levels obtained in cultures not treated with pyruvate, the effect of NaN_3 on osteoclast size was more profound, suppressing cell size to significantly lower levels.

AMPK acts as a mediator of osteoclastogenic effects of pyruvate

Since energy metabolism affects ATP levels, and AMP/ATP ratio in turn regulates AMPK, we next assessed its involvement in the pyruvate-induced osteoclastogenesis. First, we examined AMPK expression during osteoclastogenesis. AMPK consists of three subunits: AMPKα, β and γ. Activation of AMPK by AMP does not involve phosphorylation. Nevertheless, the overall capacity of a catalytic subunit AMPKα is regulated by phosphorylation. AMPKβ is a regulatory subunit, which does not appear to affect osteoclastogenesis (Quinn et al., 2010), and AMPKγ contains the AMP binding site acting as a sensor for AMP. Osteoclastic differentiation resulted in a gradual increase in the expression of AMPKα1, and a decrease in AMPKα2, AMPKβ2 and AMPKγ3 (Fig. 8A). Using immunoblotting, we confirmed the increase in AMPKα1 protein levels and increase in AMPKα1 phosphorylation (Fig. 8B), indicating change in AMPK sensitivity and/or capacity during osteoclastogenesis.

We next used RNA interference to assess the role of AMPK in regulation of osteoclastogenesis (Fig. 8C–F). Using three different siRNA oligonucleotides for AMPKα and AMPKγ, we were able to reduce the protein levels of these targets to 30–40% of control (Fig. 8C,D). Downregulation of AMPKα, which interferes with AMPK capacity, resulted in a trend toward reducing number of osteoclast-like cells and did not affect their size. In contrast, siRNAs for AMPKγ, which interfere with AMPK ability to interact with AMP, did not affect osteoclast number (Fig. 8E), but significantly increased osteoclast size (Fig. 8F). These data suggest that catalytic activity of AMPKα is important for osteoclastogenesis, while the AMP-sensing capacity of AMPKγ plays a role in regulating osteoclast growth.

AMPK is activated in energy-deficient conditions, and inhibited in energy-rich conditions. We next assessed if activation of AMPK with 5-amino-4-imidazole carboxamide ribonucleotide (AICAR) will interfere with the effects of pyruvate. Treatment with AICAR did not affect the ability of pyruvate to increase number of osteoclast-like cells (Fig. 8G), but significantly decreased cell size (Fig. 8H) to the levels observed in control cultures. AICAR also significantly reduced osteoclast numbers in control cultures, indicating that AMPK is not fully activated in control conditions in our experiments, thus implying that the control conditions are not energy deprived.

AMPK is downregulated in energy-rich conditions; therefore pharmacological AMPK inhibition is anticipated to mimic the effects of pyruvate. We have found that inhibition of AMPK with low concentrations of dorsomorphin in control cultures had a minor effect on cell number (Fig. 8I), but strongly increased size of giant osteoclast-like cells (Fig. 8J), demonstrating an induction of osteoclast growth to the levels observed in pyruvate-treated cultures.

Discussion

In this study, we have manipulated energy metabolism *in vitro* and *in vivo* by altering pyruvate levels, and have demonstrated

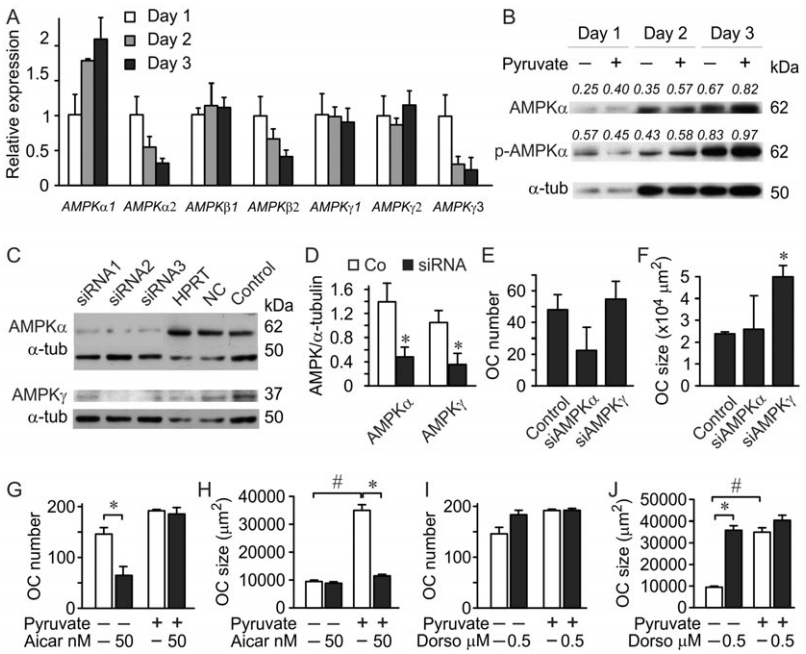

Fig. 8. AMPK pathway mediates pyruvate effects on osteoclast size. (**A**) Non-adherent bone marrow cells were treated with MCSF (50 mg/ml) and RANKL (100 ng/ml) and RNA extracts were collected on day 1, 2 and 3 after induction of differentiation. Expression of AMPKα, β and γ isoforms was normalized to the expression of GAPDH and presented relative to the level of each isoform on day 1. Data are means ± s.d., $n=3$ replicates. (**B**) RAW 264.7 cells were treated for 3 days with RANKL (50 ng/ml), with or without pyruvate (1 mM), cell lysates were collected and phospho-AMPKα, and AMPKα, were assessed by immunoblotting; α-tubulin was used as a loading control. The blot was first probed for phospho-AMPKα, stripped and then blotted for total AMPKα. The number above the blot indicates the ratio of protein levels relative to α-tubulin for AMPKα or relative to total AMPKα for phospho-AMPKα. (**C–F**) siRNA (10 nM) against AMPKα (3 different oligonucleotides) or AMPKγ (3 different oligonucleotides), a universal double scrambled negative control (NC) and a HPRT control were transiently transfected into RAW 264.7 cells, which were then treated for 4 days with RANKL (50 ng/ml) in the absence of pyruvate. (C) Cell lysates were collected from untransfected osteoclasts generated from RAW 264.7 cells (control), or from osteoclasts transfected with indicated oligonucleotides, and immunoblotted on the same membrane for AMPKα (top), or AMPKγ (bottom), α-tubulin was used as a loading control and is the same for control samples blotted for AMPKα and AMPKγ. Shown are data from one of two independent experiments, (D) average protein levels of AMPKα and AMPKγ in control samples (open bars) and samples treated with corresponding siRNA (black bars). Data are means ± s.d., $n=3$ samples treated with different oligonucleotides, $^{*}P<0.05$ indicates significance assessed by *t*-test. (E,F) Effect of siRNAs for AMPKα or AMPKγ on the osteoclasts number (E) and size (F) were assessed. Data are means ± s.d., $n=3$ samples treated with different oligonucleotides for osteoclast numbers, $n=47$–148 cells for osteoclast size, shown are data from one of two independent experiments, $^{*}P<0.05$ indicates significance assessed by *t*-test. (**G**,**H**) RAW 264.7 cells were treated for 4 days with RANKL, with or without pyruvate (1 mM), and in the absence or presence of AMPK activator AICAR (50 nM), and osteoclast number (G) and size (H) were assessed. Data are means ± s.e.m., $n=3$ independent experiments, $^{*}P<0.05$ compared to without AICAR; $^{\#}P<0.01$ compared to without pyruvate indicate significance assessed by paired *t*-test. (**I**,**J**) RAW 264.7 cells were treated for 4 days with RANKL, with or without pyruvate (1 mM), and in the absence or presence of AMPK inhibitor dorsomorphin (Dorso, 0.5 μM), and osteoclast number (I) and size (J) were assessed. Data are means ± s.e.m., $n=3$ independent experiments, $^{*}P<0.05$ compared to without dorsomorphin; $^{\#}P<0.01$ compared to without pyruvate indicate significance assessed by paired *t*-test.

that small increases in pyruvate augment osteoclastogenesis, resulting in the formation of larger and often more osteoclasts. This effect was observed in all the models of osteoclastogenesis, independent of basal glucose and pyruvate levels in the media. Addition of pyruvate augmented mitochondrial respiration, resulting in a threefold increase in ATP levels, confirming the bioenergetic nature of the effect. We identified the role of metabolic sensor AMPK in regulating osteoclast formation in energy-rich conditions. Thus, not only does cell bioenergetics change during osteoclast differentiation, but the effectiveness of energy metabolism can in turn augment osteoclastogenesis.

The surprising and important feature of our findings is that only small additions of pyruvate induce osteoclastogenesis. Moreover, addition of pyruvate led to similar changes in osteoclasts in cultures of strikingly different basal glucose and pyruvate levels. To reconcile these observations, it is important to consider the homeostatic nature of energy metabolism. Regulation of energy metabolism in the cell is tailored to providing sufficient ATP for all processes. ATP is not stored in the cell, and ATP-consuming processes are dynamic in nature. Therefore, energy production in the cell is actively adjusted for changing demands, and is determined by the levels of energy consumption, rather than extracellular concentrations of metabolic substrates (Atkinson, 1968; Ataullakhanov and Vitvitsky, 2002). Thus, at any basal glucose and pyruvate levels, cellular rates of glycolysis and oxidative phosphorylation are adapted to energy demands due to precursor proliferation, growth and fusion, and osteoclast differentiation, fusion and growth. If energy metabolism cannot provide sufficient ATP to maintain all these processes, some of them will not be accomplished (as we observed in cultures treated with the respiration inhibitor NaN_3). Conversely, when the rates of energy production prevail over the rates of energy consumption, a build-up of ATP stimulates negative feedbacks (for example, through ATP-dependent stimulation of pyruvate dehydrogenase kinase (Roche and Hiromasa, 2007)) resulting in downregulation of the

energy metabolism in the continuous presence of metabolic substrates. It is conceivable that during differentiation, a gradual increase in energy consumption provides tolerance room for an increase in energy production, so that moderate excess of energy substrates, such as pyruvate, may facilitate the realization of differentiation signaling. This logic also accounts for a bell-shaped dose-dependence of osteoclastogenesis on concentration of pyruvate.

The addition of pyruvate during osteoclastogenesis augmented cell energy metabolism, evident from an increase in medium acidification, mitochondrial activity and ATP production. Together with previous studies (Dudley and Spiro, 1961; Williams et al., 1997; Kim et al., 2007; Ishii et al., 2009; Le Nihouannen et al., 2010), these data demonstrate that osteoclast differentiation is an energy-expensive process, which requires strong upregulation of energy metabolism. Pyruvate was previously shown to protect cells from apoptosis induced by oxidative stress (Long and Halliwell, 2009). We have also observed an anti-apoptotic effect of pyruvate; however, the osteoclast redox state was affected minimally. Moreover, it was previously shown that oxidative stress supports osteoclast differentiation (Huh et al., 2006; Le Nihouannen et al., 2010), therefore the potential anti-oxidative effects of pyruvate are likely counter-productive during osteoclastogenesis. Thus, our data suggest that osteoclastogenic action of pyruvate is due to its effect on energy metabolism.

We assessed the roles of metabolic sensor AMPK in pyruvate-induced osteoclastogenesis. AMPK is directly linked to energy metabolism reflected by AMP/ATP ratio, and its activation leads to energy conservation through inhibition of cell growth, lipogenesis and protein biosynthesis (Gwinn et al., 2008; Lage et al., 2008). Inhibition of AMPK was required for osteoclast growth observed in energy-rich conditions, while activation of AMPK prevented pyruvate-induced increase in cell size. Previous report demonstrated that AMPK activator, AICAR, decreases osteoclast activity *in vitro* and *in vivo* through AMPK-dependent pathways (Quinn et al., 2010). It is known that larger osteoclasts are associated with higher resorptive activity (Trebec et al., 2007), therefore these effects may reflect decreased osteoclast size following treatment with AICAR.

Taken together, our data demonstrate the existence of reciprocal communication between the cell energy metabolism and the differentiation signaling resulting in formation of osteoclasts, cells responsible for bone destruction. These studies are important for understanding the mechanisms underlying skeletal disorders associated with diseases resulting in abnormal levels of energy metabolism substrates, such as diabetes mellitus (Nicodemus and Folsom, 2001; Kayal et al., 2007; Khazai et al., 2009) and pyruvate dehydrogenase complex deficiencies (Barnerias et al., 2010), as well as for understanding the general relationship between homeostatic and functional cellular operations.

Materials and Methods

Cell culture reagents

Fetal bovine serum (FBS) was from HyClone (SH 30396-03), MEM (11095), α-MEM (310-022-CL), DMEM (319-020-CL), pyruvate (600-110-EL), L-glutamine (609-065-EL), penicillin/streptomycin (450-201-EL), trypsin/ethylenediamine tetraacetic acid (T/E, 325-042-EL) were from Wisent Inc. L-ascorbic acid (A5960), and Sodium azide (S2002) were from Sigma–Aldrich Co. Dorsomorphin 2HCl (3093) and AICAR (2840) were from TOCRIS bioscience. Recombinant human M-CSF (300-25) was from Peprotech Inc. Recombinant glutathione S-transferase-soluble RANKL was purified from the clones kindly provided by Dr M.F. Manolson (University of Toronto).

In vivo study

All animal studies were performed in accordance with the McGill University animal care guidelines established by the Canadian Council on Animal Care. Six-week-old C57BL6/J mice (Charles River) received 0.75 g/kg/day of pyruvate solution or sterile saline by daily i.p. injections for 6 days. On day 7, 24 hours after the last injection, blood samples were collected and the long bones were isolated. Six-hour fasted blood levels of glucose and pyruvate were evaluated using an Accu-chek Aviva glucometer and EnzyChrom™ Pyruvate Assay Kit (BioAssay Systems, EPYR-100). Bone samples were embedded in paraffin and 5 μm sections were stained for tartrate-resistant acid phosphatase (TRAP). Osteoclast analysis in bone sections was conducted using Osteomeasure software (Osteometrics Inc., Atlanta GA).

Osteoclast cultures from mouse bone marrow cells

Mouse bone marrow cells were collected from six-week-old C57BL6/J mice (Charles River) for total bone marrow cultures or BALB/c mice (Charles River) for non-adherent bone marrow cultures as described previously (Tiedemann et al., 2009). For total bone marrow cultures, cells were plated at a density of 2.5×10^6 cells/cm^2 and cultured in MEM supplemented with 1% penicillin–streptomycin and 10% FBS in the presence of RANKL (50 ng/ml) and AA (50 μg/ml). For non-adherent bone marrow cultures, cells were first cultured in 75 cm^2 tissue culture flasks (15×10^6 cells per flask) with M-CSF (25 ng/ml). On day 1, non-adherent cells were removed, resuspended in α-MEM with M-CSF (50 ng/ml) and RANKL (100 ng/ml), and plated at 7×10^4 cells/cm^2. Medium was changed every second day.

RAW 264.7 monocyte cell culture

RAW 264.7 cells (ATCC) were cultured in 25 cm^2 tissue culture flasks in DMEM supplemented with 1% penicillin–streptomycin and 10% FBS. To generate osteoclasts, RAW 264.7 cells were plated at 10^4 cells/cm^2. On days 1 and 3, medium was changed and RANKL (50 ng/ml) was added.

Characterization of osteoclasts

Cell cultures were fixed using 4% paraformaldehyde and stained for TRAP (Sigma–Aldrich Co., 387A). Osteoclasts were identified as multinucleated (more than 3 nuclei) TRAP-positive cells and were further characterized by image analysis using PixeLINK Capture SE® software (PixeLINK) and Image J. For each experimental condition, the cell surface area and nuclei number of ~100 osteoclasts were evaluated. For confocal microscopy, live osteoclasts generated from RAW 264.7 cells on glass coverslips were incubated with the fluorescent lipophilic membrane probe DiI (5 μl/ml, Vybrant® DiI, Invitrogen™, V-22885), and visualized with LSM510 confocal microscope (Carl Zeiss Inc.). Images of at least 20 fields/condition were used to evaluate osteoclast height.

Cell proliferation assay

RAW 264.7 cells cultured for 24 hours in 96-well flat bottom plates were supplemented with indicated additions, and cultured for 48 hours. Proliferation assay was performed using the BrdU CHEMICON® Cell Proliferation Assay Kit (Millipore, 2750) and a microplate reader (Beckman Coulter AD340, Beckman Coulter Inc.).

Apoptosis assay

RAW 264.7 cells plated on glass coverslips, were treated as indicated, fixed and stained using DAPI dihydrochloride (Invitrogen™, D1306). Ten random images per condition were collected in each experiment, each image containing 8–25 precursors. Nuclei were rated positive for apoptosis if they exhibited condensation and a loss of membrane integrity. The rate of apoptosis was estimated as a proportion of cells demonstrating nuclear fragmentation from the total number of cells analyzed.

Resorption assay

RAW 264.7 cells were plated on mineral-coated Osteoassay Plates (Corning Inc., 3988), osteoclast formation was induced by treatment with RANKL for five days, after which the experimental treatments were applied for an additional five days. Plates were washed with diluted bleach to remove cells, and air-dried. Resorption pits were counted and the planar area of each pit was measured by using a Nikon ECLIPSE TS100 microscope coupled to a Nikon ELWD 0.3 T1-SNCP camera and PixeLINK Capture SE image-analysis software.

Mitochondrial activity

RAW 264.7 cells were plated on 10 mm diameter glass coverslips. Mitochondrial activity was assessed using 5,5′,6,6′-tetrachloro-1,1′,3,3′-tetraethylbenzimidazolylcarbocyanine iodide (JC-1; CBIC2(3), Invitrogen™, T-3168) as described previously (Komarova et al., 2000). In each experiment, images of at least 9 fields were collected, the background fluorescence in red and green channel was subtracted from the

images. All positively stained particles were then selected and filtered to remove very small and very large items and the ratio of the average fluorescence intensity of the red channel to the average fluorescence intensity of the green channel was identified.

Protein extraction and immunoblotting

Cell lysates were extracted in RIPA lysis buffer containing 50 mM Tris, pH 7.4, 150 mM NaCl, 1% Nonidet P-40, 1 mM EDTA, 1 mg/ml aprotinin, 2 mg/ml leupeptin, 0.1 mM phenylmethylsulfonyl fluoride, 20 mM sodium fluoride, 0.5 mM sodium orthovanadate and centrifuged at 12,000 g for 10 minutes at 4℃. Supernatant was collected, and protein was measured using a Quant-iT^{TM} protein assay kit (Invitrogen). 20–40 µg of lysates was separated on a 7.5% or 12% SDS-PAGE and transferred to a nitrocellulose membrane (0.45 µm, 162-0115, Bio-Rad) using 10 mM sodium borate buffer. The membranes were blocked in 5% milk in TBST buffer (10 mM Tris-HCl, pH 7.5, 150 mM NaCl, 0.05% Tween 20) for 1 hour at room temperature, and incubated overnight at 4℃ with primary antibodies: AMPKα1 (1:1000, 2603, Cell Signaling), p-AMPKα1 (1:1000, 2535, Cell Signaling), AMPKγ1 (1:1000, 4187, Cell Signaling) and α-tubulin (1:5000, T9026, Sigma). The blots were visualized with horseradish peroxidase-conjugated secondary antibodies (anti-rabbit, 170-5046; anti-mouse, 170-5047 Bio-Rad) and a chemiluminescence system (Super signal West Pico; 34080, Pierce).

RNA isolation and RT-PCR

Total RNA was isolated from primary cultures using the RNeasy mini kit and QIAshredder columns (Qiagen, 74104 and 79654). For real-time PCR, 1 µg of total RNA was reverse transcribed using a cDNA archive kit (Applied Biosystems, 74322171). Real-time PCR was performed using 7500 Applied Biosystems instrument, with TaqMan Universal PCR Master Mix (Applied Biosystems, 4304437) and the following TaqMan gene expression assays: MMP-9 (Mm00600163_m1), cathepsin K (Mm00484036_ m1), calcitonin receptor (Mm00432271_m1) and β-actin (Mm00607939_s1). Real-time PCR for PRKaa, PRKaa2, PRKab1, PRKab2, PRKay1, PRKay2, PRKay3 and GAPDH was performed using SYBR Green Universal PCR Master Mix (Applied Biosystems, 4367659) and the following primers: PRKaa forward 5′-AGAGGGCCGCAATAAAAGAT-3′, and reverse 5′-TGTTGTACAGGCAGCTGAGG-3′; PRKaa2 forward 5′-TGGCTGCCTTCTTATGCTTT-3′, and reverse 5′-GCTTTGAAACGGCTTCTCAC-3′; PRKab1 forward 5′-TCCGATGTGTCTGAGCTGTC-3′, and reverse 5′-CAGTGCTGGGTCACAAGAGA-3′; PRKab2 forward 5′-GTGATGTGACGTGGAAGTGG-3′, and reverse 5′-GCAAGAACTTGGCTTTGAGG-3′; PRKay1 forward 5′-TCGGTCCCACTACTTTGAGG-3′, and reverse 5′-GATGTCAGACAGCGAAACGA-3′; PRKay2 forward 5′-GCCTTATGTCCAAACGCAAT-3′, and reverse 5′-AGCGCTTAGAGGCATCACAT-3′, PRKay3 forward 5′-CCACGAGAGCCTAGGTGAAG-3′ and reverse, 5′-TTCCAAGATCCTTTCGTTGG-3′; and GAPDH forward, 5′-TTCCGTGTTCCTACCCCCAA-3′, and reverse, 5′-GATGCCTGCTTCACCACCTT-3′.

siRNA against AMPKα1 and AMPKγ1

Short interfering RNAs for AMPKα1 (5′-GGAAUCCUCAUAGACCUUAUUAGAT-3′ and 5′-AUCUAAUAAGGUCUAUGAGGAUUCCAG-3′), (5′-GGAGGAGCCAACUAAAUAGGACCTT-3′ and 5′-AAGGUCCUAUUUAGUUGGCUCCUCCUU-3′), (5′-CCAAUCCAGUGCAUAGAAAGGACAG-3′ and 5′-CUGUCCUUUCUAUGCACUGGAUUGGCU-3′) and AMPKγ1 (5′-ACUCCACCUAAGAUAAUAGCUCUGC-3′ and 5′-GCAGAGCUAUUAUCUUAGGUGGAGUAA-3′), (5′-AGCCGGAAUUCAUGUCUAAGUCUCT-3′ and 5′-AGAGACUUAGACAUGAAUUCCGGCUUG-3′), (5′-ACAAGAUAGAGACGUGGAGAGAGGT-3′ and 5′-ACCUCUCUCCACGUCUCUAUCUUGUGC-3′), as well as an hypoxanthine guanine phosphoribosyl transferase (HPRT) RNA interference duplex (5′-GCCAGACUUUUUGGAUUUGAAATT-3′ and 5′-AAUUUCAAAUCCAACAAAGUCUGGCUU-3′), and negative control double scrambled RNA interference duplex (5′-CGUAAUCGCGUAAUUUACGCGUAT-3′ and 5′-AUACGCGUAUUAUACGCGAUUAACGAC-3′) were purchased from Integrated DNA Technologies (TriFECTa NM_001013367 and NM_016781). RAW 264.7 cells were cultured for 24 hours, then the medium was changed to medium without antibiotics, and 1 hour later RANKL was added and transfection was performed using Lipofectamine 2000 (Invitrogen, 11668-019) with 10 nM of duplex. Protein lysates were taken at day 2 to confirm the efficiency of AMPKα1 and AMPKγ1 knockdown. For osteoclastogenesis experiments, on day 5 after transfection osteoclasts were fixed and analyzed as described.

Measurements of pH, lactate, ATP, total and oxidized glutathione

RAW 264.7 cells were plated in 6-well plates and supplemented with fresh medium containing indicated additions on days 1 and 3. On days 3 and 5, pH of the medium was measured with an electronic pH meter (Accumet® Basic AB15, Fisher scientific). On day 5, cell culture media were collected and precipitated with perchloric acid and neutralized with KOH. Supernatants of samples were processed for lactate determination using EnzyChrom^{TM} L-lactate assay kit (BioAssay Systems, ECLC-100) and microplate reader (Tecan's Infinite® F200, Tecan US Inc.). ATP levels were measured by the luciferin–luciferase method using an ATP Determination Kit (Invitrogen^{TM}, A22066) and a luminometer (Femtomaster FB12, Zylux Corp.). GSHt and GSSG were measured using a GSH/GSSH Assay Kit (Oxford Biomedical Research^{TM}, GT35) and microplate reader (Tecan's Infinite® F200). ATP and GSHt concentrations were normalized to the protein content measured using a Quant-iT^{TM} protein assay kit (Invitrogen).

Statistical analysis

Data are presented as representative images, representative experiments or as means ± standard error of the mean, with n indicating the number of independent experiments. Differences were assessed by ANOVA for correlated samples followed by Tukey post-test, Student t-test, or paired Student t-test as indicated in the figure legends and accepted as statistically significant at $P<0.05$.

Acknowledgements

We thank Dr M.F. Manolson, University of Toronto for providing reagents used in this study and Xiaomin Yu for her help in acquisition of preliminary data. This study was supported by the Canadian Institute for Health Research. D.L.N. was supported by the CIHR Training Program in Skeletal Health Research, the Canadian Arthritis Network and les Fonds de la Recherche en Santé du Québec. J.E.F. was supported by the CIHR Training Program in Skeletal Health Research and McGill University. J.E.B. holds Canada Research Chair in Osteoinductive Biomaterials and S.V.K. holds Canada Research Chair in Osteoclast Biology.

Competing Interests

The authors have no competing interests to declare.

References

Ataullakhanov, F. I. and Vitvitsky, V. M. (2002). What determines the intracellular ATP concentration. *Biosci. Rep.* **22**, 501-511.

Atkinson, D. E. (1968). The energy charge of the adenylate pool as a regulatory parameter. Interaction with feedback modifiers. *Biochemistry* **7**, 4030-4034.

Barnerias, C., Saudubray, J. M., Touati, G., De Lonlay, P., Dulac, O., Ponsot, G., Marsac, C., Brivet, M. and Desguerre, I. (2010). Pyruvate dehydrogenase complex deficiency: four neurological phenotypes with differing pathogenesis. *Dev. Med. Child Neurol.* **52**, e1-e9.

Bassenge, E., Sommer, O., Schwemmer, M. and Bünger, R. (2000). Antioxidant pyruvate inhibits cardiac formation of reactive oxygen species through changes in redox state. *Am. J. Physiol.* **279**, H2431-H2438.

Czupalla, C., Mansukoski, H., Pursche, T., Krause, E. and Hoflack, B. (2005). Comparative study of protein and mRNA expression during osteoclastogenesis. *Proteomics* **5**, 3868-3875.

Dudley, H. R. and Spiro, D. (1961). The fine structure of bone cells. *J. Biophys. Biochem. Cytol.* **11**, 627-649.

Finley, L. W. and Haigis, M. C. (2009). The coordination of nuclear and mitochondrial communication during aging and calorie restriction. *Ageing Res. Rev.* **8**, 173-188.

Fukushima, M., Lee, S. M., Moro, N., Hovda, D. A. and Sutton, R. L. (2009). Metabolic and histologic effects of sodium pyruvate treatment in the rat after cortical contusion injury. *J. Neurotrauma* **26**, 1095-1110.

Gwinn, D. M., Shackelford, D. B., Egan, D. F., Mihaylova, M. M., Mery, A., Vasquez, D. S., Turk, B. E. and Shaw, R. J. (2008). AMPK phosphorylation of raptor mediates a metabolic checkpoint. *Mol. Cell* **30**, 214-226.

Huh, Y. J., Kim, J. M., Kim, H., Song, H., So, H., Lee, S. Y., Kwon, S. B., Kim, H. J., Kim, H. H., Lee, S. H. et al. (2006). Regulation of osteoclast differentiation by the redox-dependent modulation of nuclear import of transcription factors. *Cell Death Differ.* **13**, 1138-1146.

Ishii, K. A., Fumoto, T., Iwai, K., Takeshita, S., Ito, M., Shimohata, N., Aburatani, H., Taketani, S., Lelliott, C. J., Vidal-Puig, A. et al. (2009). Coordination of PGC-1β and iron uptake in mitochondrial biogenesis and osteoclast activation. *Nat. Med.* **15**, 259-266.

Kayal, R. A., Tsatsas, D., Bauer, M. A., Allen, B., Al-Sebaei, M. O., Kakar, S., Leone, C. W., Morgan, E. F., Gerstenfeld, L. C., Einhorn, T. A. et al. (2007). Diminished bone formation during diabetic fracture healing is related to the premature resorption of cartilage associated with increased osteoclast activity. *J. Bone Miner. Res.* **22**, 560-568.

Khazai, N. B., Beck, G. R., Jr and Umpierrez, G. E. (2009). Diabetes and fractures: an overshadowed association. *Curr. Opin. Endocrinol. Diabetes Obes.* **16**, 435-445.

Kim, J. M., Jeong, D., Kang, H. K., Jung, S. Y., Kang, S. S. and Min, B. M. (2007). Osteoclast precursors display dynamic metabolic shifts toward accelerated glucose metabolism at an early stage of RANKL-stimulated osteoclast differentiation. *Cell. Physiol. Biochem.* **20**, 935-946.

Komarova, S. V., Ataullakhanov, F. I. and Globus, R. K. (2000). Bioenergetics and mitochondrial transmembrane potential during differentiation of cultured osteoblasts. *Am. J. Physiol. Cell Physiol.* **279**, C1220-C1229.

Lage, R., Diéguez, C., Vidal-Puig, A. and López, M. (2008). AMPK: a metabolic gauge regulating whole-body energy homeostasis. *Trends Mol. Med.* **14**, 539-549.

Le Nihouannen, D., Barralet, J. E., Fong, J. E. and Komarova, S. V. (2010). Ascorbic acid accelerates osteoclast formation and death. *Bone* **46**, 1336-1343.

Lee, Y. S., Kim, Y. S., Lee, S. Y., Kim, G. H., Kim, B. J., Lee, S. H., Lee, K. U., Kim, G. S., Kim, S. W. and Koh, J. M. (2010). AMP kinase acts as a negative regulator of RANKL in the differentiation of osteoclasts. *Bone* **47**, 926-937.

Long, L. H. and Halliwell, B. (2009). Artefacts in cell culture: pyruvate as a scavenger of hydrogen peroxide generated by ascorbate or epigallocatechin gallate in cell culture media. *Biochem. Biophys. Res. Commun.* **388**, 700-704.

Mohanty, I., Joshi, S., Trivedi, D., Srivastava, S., Tandon, R. and Gupta, S. K. (2002). Pyruvate modulates antioxidant status of cultured human lens epithelial cells under hypergalactosemic conditions. *Mol. Cell. Biochem.* **238**, 129-135.

Nicodemus, K. K. and Folsom, A. R. (2001). Type 1 and type 2 diabetes and incident hip fractures in postmenopausal women. *Diabetes Care* **24**, 1192-1197.

Quinn, J. M., Tam, S., Sims, N. A., Saleh, H., McGregor, N. E., Poulton, I. J., Scott, J. W., Gillespie, M. T., Kemp, B. E. and van Denderen, B. J. (2010). Germline deletion of AMP-activated protein kinase β subunits reduces bone mass without altering osteoclast differentiation or function. *FASEB J.* **24**, 275-285.

Roche, T. E. and Hiromasa, Y. (2007). Pyruvate dehydrogenase kinase regulatory mechanisms and inhibition in treating diabetes, heart ischemia, and cancer. *Cell. Mol. Life Sci.* **64**, 830-849.

Tiedemann, K., Hussein, O., Sadvakassova, G., Guo, Y., Siegel, P. M. and Komarova, S. V. (2009). Breast cancer-derived factors stimulate osteoclastogenesis through the Ca^{2+}/protein kinase C and transforming growth factor-β/MAPK signaling pathways. *J. Biol. Chem.* **284**, 33662-33670.

Trebec, D. P., Chandra, D., Gramoun, A., Li, K., Heersche, J. N. and Manolson, M. F. (2007). Increased expression of activating factors in large osteoclasts could explain their excessive activity in osteolytic diseases. *J. Cell. Biochem.* **101**, 205-220.

Wild, S., Roglic, G., Green, A., Sicree, R. and King, H. (2004). Global prevalence of diabetes: estimates for the year 2000 and projections for 2030. *Diabetes Care* **27**, 1047-1053.

Williams, J. P., Blair, H. C., McDonald, J. M., McKenna, M. A., Jordan, S. E., Williford, J. and Hardy, R. W. (1997). Regulation of osteoclastic bone resorption by glucose. *Biochem. Biophys. Res. Commun.* **235**, 646-651.